

Regular Article

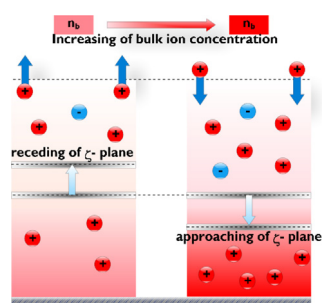
Flexibility of inactive electrokinetic layer at charged solid-liquid interface in response to bulk ion concentration

Amer Alizadeh, Moran Wang*

Department of Engineering Mechanics and CNMM, Tsinghua University, Beijing 100084, China



GRAPHICAL ABSTRACT



ARTICLE INFO

Article history:

Received 1 July 2018

Revised 31 August 2018

Accepted 3 September 2018

Available online 06 September 2018

Keywords:

Zeta potential plane

Inactive electrokinetic layer

Electrical quad-layer model

Ionic conductivity

Narrow nanochannels

ABSTRACT

It has been a long-lasting debate on the position of zeta potential plane within aqueous solutions. This paper reports a flexible behavior of the inactive electrokinetic layer between the outer-Helmholtz plane and zeta potential plane, so-called buffer layer, in response to bulk ion concentration. This flexibility is not only corroborated by analyzing the measured zeta potentials with resulting electrical quad-layer model (inner- and outer-Helmholtz, buffer, and diffuse layers) but also consistent with thermodynamic analysis. The model indicates that the flexible buffer layer thickness saturates to its minimum for concentrated solutions. The predicted ionic conductance agrees well with the previous experimental measurements in nanochannels. The theory provides a deep physical insight into understanding, design, and manipulation of ion transport in nanosystems.

© 2018 Elsevier Inc. All rights reserved.

1. Introduction

Ion transport through nanoscale biological ion channels and porous membranes has been the source of biomimetics for fabrication and investigation of artificial nanochannels in nanofluidics [1–17]. The solid-aqueous interface of the fabricated nanochannels may acquire surface charge owing to specific adsorption or desorption of the dissolved ions [18,19]. In response to positive or negative acquired surface charge, the long-range Coulomb interaction

imposes attraction and repulsion forces on the counter- and co-ions, respectively. Possible arrangements of ions at the vicinity of the charged solid surface has been a subject of investigation for decades [20,21]. The experimental measurements of the electrokinetic surface charge density (σ^{ele}) compared with the surface charge density (σ^0) unveiled a small fraction of the countercharges contribute in ion transfer through the charged channel [22]. This observation eventuated to a hypothesis that the electric double layer may be formed as hydrodynamic immobile and mobile layers at which a significant portion of the counter-ions is embedded in the immobile layer and does not contribute in the zeta potential measurements (electrophoretic, electroosmotic or streaming

* Corresponding author.

E-mail address: mrwang@tsinghua.edu.cn (M. Wang).

potential). Following this hypothesis, Eversole and co-workers [23,24] proposed a rigid structure for the immobile layer in which the thickness of this layer was determined based on the measured zeta potential. The main shortcoming of their theory was that the electric potential on the solid surface was assumed to be independent of bulk ion concentration. Bikerman [25] challenged the existence of immobile layer by stating no reasonable interpretation for the existence of this layer from the hydrodynamic or electrostatic point of view. They argued that the immobile layer, in principle, represented roughness of solid surface where solution within cavities of the surface could barely move via the shear or electrostatic forces. In contrast to the Bikerman, Lyklema and Overbeek [26] proposed the electroviscous effects as the origin of immobile layer. Later, Lyklema et al. [22] demonstrated that neither the roughness of charged surface nor the electroviscous effects would be adequate to interpret discrepancy between the measured σ^{ele} and σ^0 because, for very smooth and homogeneous surfaces like mercury, the effects of the immobile layer could still be detected. They conducted a classical molecular dynamics (MD) simulation with which a gel-like feature of fluid at the vicinity of the solid surface was reported regardless of presence or absence of surface charge. Very recently, McMullen and co-workers revealed that in order to interpret the anomalous finding of translocation of charged filamentous viruses in nanopores one has to consider the presence of stagnant boundary layer at the vicinity of nanopore walls. They showed that the changes in extent of the stagnant layer depended on the bulk ion concentration [27]. Lyklema [28] proposed that from a physical point of view, only the solution beyond the zeta potential plane (slipping or shear plane) is electrokinetically active. Predota et al. [29] conducted a MD simulation to shed light on the origin of the zeta potential. They found that the origin of zeta potential was not due to the presence of a slipping plane which separated the mobile and immobile layer in the vicinity of the solid-liquid interface. In contrast, the zeta potential arises from the electrokinetically driven motion of ions within an imbalanced charge layer within 1.5 (nm) to 2.0 (nm) of the surface. Although their results took a long step forward to understand the origin of the zeta potential, however, an independent surface charge from the bulk ion concentration and solution pH was the main defect of MD simulations.

Despite the all aforementioned efforts, the location of the zeta potential plane has not been comprehended appropriately yet

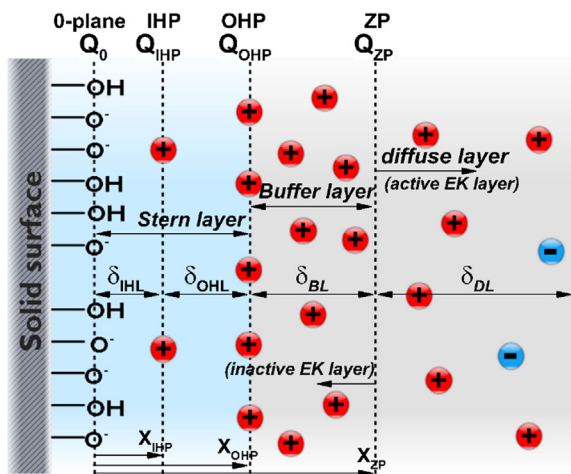


Fig. 1. The configuration of the proposed electrical quad-layer (EQL) model. The buffer layer (BL) represents the distance from the outer-Helmholtz plane (OHP) to zeta potential plane (ZP). The diffuse layer (DL) starts from ZP to bulk solution. The four layers, inner-Helmholtz layer (IHL), outer-Helmholtz layer (OHL), BL, and DL postulate three series differential capacitors. The active and inactive electrokinetic (EK) layers are depicted as the solution beyond and underneath of ZP, respectively.

since the slipping plane theory is recognized to be an abstraction of reality [29,30]. In this contribution, we analyze the position of zeta potential plane and find that it has a reciprocal relation with the bulk ion concentration. To model the position of the zeta potential plane, we develop a phenomenological electrical quad-layer (EQL) model, as shown in Fig. 1, with a flexible buffer layer (FBL) to bridge the diffuse and Stern layers. The proposed EQL model could unveil the physics underlying of ion transport through very narrow nanochannels.

2. Theoretical method

The available electric double layer theories work well for most electrokinetic transport in large scale cases, but fail to interpret the position of zeta potential plane and consequently the ionic transport at very narrow nanochannels (lower than 4 nm) [31,32]. For instance, the electrical triple-layer model (TLM) predicts a non-physical distance (about 3 nm) between IHP and OHP [33]. In order to propose a near-to-reality surface complexation model to interpret the position of zeta potential plane, we assume the presence of a buffer layer (BL) which has interface with the diffuse layer (DL) and outer-Helmholtz layer (OHL) at the zeta potential plane (ZP) and outer-Helmholtz plane (OHP), respectively (Fig. 1). The BL, in fact, could be the outcome of the stagnant layer [22,28], electroviscous effects [26] or a complex interplay of the electrostatics, structure, and spatially varying dynamics [29] at the vicinity of OHP. We note that from a molecular point of view, there is no any distinguishable plane within the electric double layers. However, from the macroscopic standpoint, the solution layers with different electrostatic and hydrodynamic features can be distinguished by means of hypothetical planes.

2.1. Surface complexation models with flexible buffer layer

The thermodynamic analysis unveils a substantial fact that the thickness of BL, and subsequently the position of the zeta potential plane, behaves flexible in response to the bulk ion concentration (Fig. 2a) (Appendix A). To quantify this behavior of the buffer layer, we develop a surface complexation quad-layer model (inner- and outer-Helmholtz layer, buffer layer, and diffuse layer, Fig. 1) which employs to silica surface for sake of obtaining the thickness of buffer layer (δ_{BL}) to analyze the measured zeta potential for KCl [21,34] and NaCl [35] solutions. Moreover, in order to demonstrate that the flexibility of the BL is not a specific phenomenon to the silica-aqueous interface, we will develop an EQL model for TiO₂-aqueous interface to investigate the BL for different solid-liquid interfaces.

2.1.1. EQL model for SiO₂-aqueous solution interface

Naturally, the silica surface acquires electric charge due to the chemical adsorption of ions in the solution. In the pH range of 3–9, the typical chemical reactions of the surface adsorption at the silica surface are derived as [36]



Based on the law of mass action, the reaction equilibrium constants for the chemical adsorptions are [36]

$$K_{a1}^{\text{int}} = \frac{\sigma_{\text{SiOH}}}{\sigma_{\text{SiOH}_2^+}} n_{b,\text{H}^+} \exp(-\psi_0), \quad (4)$$

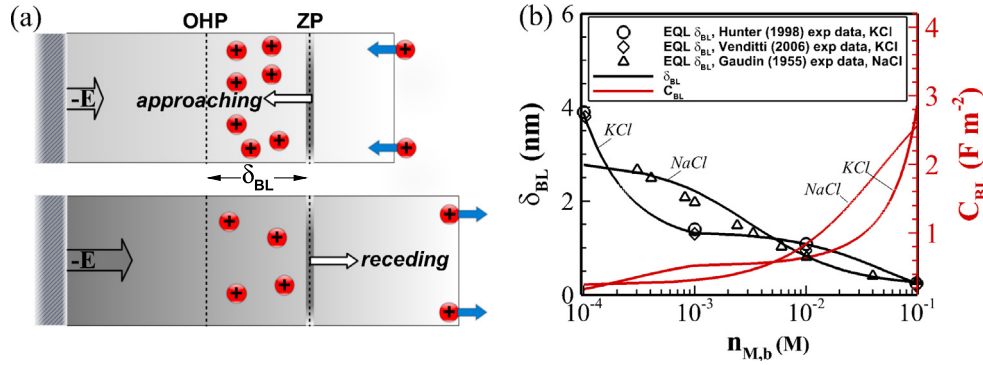


Fig. 2. (a) Our thermodynamic analysis (Appendix A) which is based on the equilibrium state (Gibbs-Duhem equation at constant pressure and temperature) for DL and BL as two systems in contact reveals the flexibility of BL. It is found that when bulk ion concentration increases ($dn_{M,b} > 0$) the ZP approaches (so-called *approaching*) toward the solid surface ($d\delta_{BL} < 0$) and recedes (so-called *receding*) to the bulk solution ($d\delta_{BL} > 0$) by decreasing the bulk ion concentration ($dn_{M,b} < 0$). (b) The best-fitted δ_{BL} for KCl solution with experimental data from Venditti et al. [34] (diamond symbol) and Hunter [21] (circle symbol) and NaCl solution with experimental data from Gaudin and Fuerstenau (triangle symbol) [35] compared with what Eq. (19) predicts for δ_{BL} (solid lines). The differential capacitance of the BL (C_{BL} , dashed lines) is obtained by $\epsilon_0 \epsilon_r \delta_{BL}^{-1}$.

$$K_{a2}^{int} = \frac{\sigma_{SiO^-}}{\sigma_{SiOH}} n_{b,H^+} \exp(-\bar{\psi}_0), \quad (5)$$

$$K_M^{int} = \frac{\sigma_{SiOM}}{\sigma_{SiO^-}} \frac{1}{n_b} \exp(\bar{\psi}_{IHP}), \quad (6)$$

where σ denotes the surface charge density (C/m^2), ψ the electric potential and T the temperature. Considering the total number of the site density as $\Gamma^0 = 5 \text{ (nm}^{-2}\text{)}$, the principle of electric charge continuity for the surface charge density eventuates to [33]

$$e\Gamma^0 = \sigma_{SiOH} + \sigma_{SiO^-} + \sigma_{SiOH_2^+} + \sigma_{SiOM}. \quad (7)$$

On the other hand, the surface charge density at silica-aqueous solution interface for four planes (Fig. 1) of 0, IHP, OHP, and ZP could be written as

$$Q_0 = \sigma_{SiOH_2^+} - \sigma_{SiO^-} - \sigma_{SiOM}, \quad (8)$$

$$Q_{IHP} = \sigma_{SiOM}, \quad (9)$$

$$Q_{OHP} = -\sqrt{8\epsilon_0 \epsilon_r k_B T n_{s,b}} \sinh(0.5\bar{\psi}_{OHP}) - Q_{ZP}, \quad (10)$$

$$Q_{ZP} = -\sqrt{8\epsilon_0 \epsilon_r k_B T n_{s,b}} \sinh(0.5\bar{\psi}_{ZP}), \quad (11)$$

where $n_{s,b}$ is the effective bulk number density of the counter-ions plus hydronium (m^{-3}) which is related to the effective bulk ionic molar concentration as

$$n_{s,b} = 1000 N_A (n_b + n_{b,H^+}), \quad (12)$$

where N_A denotes the Avogadro constant. Regarding the surface charge on the OHP, borrowing the idea of the Grahame's equation, we define

$$Q_{OHP} = \int_{X_{OHP}}^{X_{ZP}} \rho_e dx = -\epsilon_0 \epsilon_r \int_{X_{OHP}}^{X_{ZP}} \frac{d}{dx} \left(\frac{d\psi}{dx} \right) dx = -\epsilon_0 \epsilon_r \left. \frac{d\psi}{dx} \right|_{X_{OHP}}^{X_{ZP}}. \quad (13)$$

Based on the definition of the surface charge on the ZP, Eq. (13) gives rise to

$$Q_{OHP} = -\epsilon_0 \epsilon_r \left. \frac{d\psi}{dx} \right|_{X_{OHP}} - Q_{ZP}, \quad (14)$$

where if we introduce the Grahame's equation to Eq. (14) one finally has Eq. (10). Furthermore, the global electro-neutrality within the quad-layers leads to:

$$Q_0 + Q_{IHP} + Q_{OHP} + Q_{ZP} = 0. \quad (15)$$

Considering the presence of the quad-layers where extend from the solid-liquid interface to the bulk solution, one can postulate the quad-layers as three series differential capacitors

$$\psi_0 - \psi_{IHP} = \frac{Q_0}{C_{IHP}}, \quad (16)$$

$$\psi_{IHP} - \psi_{OHP} = -\frac{Q_{OHP}}{C_{OHP}}, \quad (17)$$

$$\psi_{OHP} - \psi_{ZP} = -\frac{Q_{ZP}}{C_{BL}}, \quad (18)$$

where C_{IHP} , C_{OHP} , and C_{BL} ($F m^{-2}$) are the integral differential capacities of the inner and outer parts of the Helmholtz layer, and the buffer layer, respectively, which are assuming constant in the region between planes [37]. Eqs. (4–12) and Eqs. (15–18) are formed a set of non-linear coupled equations for the EQL model. In this contribution, the constant parameters for the EQL model are considered based on the type of solution under consideration (Table 1).

For both solutions, we assumed that, $pH_{PZC} = 2.5$, and $K_{a1}^{int} = 2pH_{PZC} - \log(K_{a2}^{int})$ while the unknown parameters Q_0 , Q_{IHP} , Q_{OHP} , Q_{ZP} , ψ_0 , ψ_{IHP} , ψ_{OHP} , ψ_{ZP} will be obtained by solving the set of equations numerically. Herein, we should note that the system of EQL model's equations has not been closed yet since the BL thickness and consequently the buffer layer capacitance are remained unknown. In the equation of the capacitance of BL and diffuse layers, the $\epsilon_r = 78.54$ represents the permittivity of the water at room temperature relative to the permittivity of the vac-

Table 1
The constant parameters for the FLM.

Electrolyte solution	NaCl	KCl
$\epsilon_{r,IHL}$	22.418 ^a	16.1717 ^a
C_{IHP}	0.78 ($F m^{-2}$)	1.44 ($F m^{-2}$)
C_{OHP}	1.9 ($F m^{-2}$)	2.78 ($F m^{-2}$)
$\log K_{a2}^{int}$	-7.4 ^b	-6.64 ^b
$\log K_M^{int}$	-0.25 ^b	-0.3 ^b
ion radius(r)	0.183 (nm) ^c	0.125 (nm) ^c

^a The relative permittivity of the IHL [33] with respect to the permittivity of vacuumed space ϵ_0 .

^b The equilibrium constants for chemical reactions [33].

^c The Stokes radius of the hydrated ions [33].

uum. To close the system of equations, we define the thickness of BL phenomenologically.

Our modeling results suggest a reciprocal relation between BL thickness and bulk ion concentration as

$$\begin{aligned} a) \delta_{BL} &= \left(\frac{1}{a_1 n_{M,b} + b_1} + e_1 \right), \quad n_{M,b} < 10^{-3}, \\ b) \delta_{BL} &= \left(\frac{1}{a_2 n_{M,b} + b_2} + e_2 \right), \quad n_{M,b} \geq 10^{-3} \end{aligned} \quad (19)$$

in accordance with what we found by thermodynamic analysis. $n_{M,b}$ in Eq. (19) is the molar ion concentration of the bulk solution. Coefficients $a_{1,2}$ to $e_{1,2}$ are defined based on the solute under consideration (For *KCl* we have $a_1 = 3.809 \times 10^{12}$, $b_1 = -25 \times 10^6$, $e_1 = 1.05 \times 10^{-9}$, $a_2 = 1.12 \times 10^{10}$, $b_2 = 59 \times 10^7$, $e_2 = -3.4 \times 10^{-10}$ and for *NaCl* $a_1 = a_2 = 1.18 \times 10^{11}$, $b_1 = b_2 = 3.75 \times 10^8$, $e_1 = e_2 = 1.9 \times 10^{-10}$), whereas they are independent of the bulk ion concentration. Regarding the differential capacitance of the BL, one can figure out $C_{BL} = \epsilon_0 \epsilon_r \delta_{BL}^{-1}$, which is a function of bulk ion concentration (Fig. 2b). As Fig. 2b shows, it is interesting to note that δ_{BL} decreases dramatically by increasing the bulk ion concentration when $n_{M,b} < 10^{-3}$ (M) while decreasing slightly for $n_{M,b} > 10^{-3}$ (M) and finally saturates for concentrated solutions ($n_{M,b} \rightarrow \infty$). For both solutions, at a low bulk ion concentration, ZP recedes to the bulk solution where $\delta_{BL} > 2$ (nm). However, when we increase the bulk ion concentration, for instance $n_{M,b} = 10^{-1}$ (M), ZP approaches toward OHP and therefore $\delta_{BL} < 1$ (nm). Approaching of ZP to OHP and saturation of δ_{BL} for concentrated solution reveals a significant feature of the electric double layer when BL vanishes because of δ_{BL} which is even smaller or in order of ion's Stokes radius.

Employing the proposed EQL model to predict the acquired surface charge at the silica-aqueous solution interface shows that the EQL model predicts good agreement zeta potential (Fig. 3a and b) versus bulk ion concentration for *KCl* [34,38] and *NaCl* [35] solution

with the available experimental measurements. Moreover, since the acquired surface charge and zeta potential could be changed significantly by solution pH, we have examined the EQL model to predict the zeta potential and surface charge of the silica surface. Fig. 4 demonstrates that the EQL model predicts good agreement zeta potential and surface charge (Q_0) versus solution pH in comparison with the available experimental measurements [39]. In conclusion, in this section, we have shown that to remove the unphysical interpretation of the available EDL models, a flexible buffer layer could be added to bridge the Stern and diffuse layers where the thickness of this layer determined the position of the zeta potential plane.

2.1.2. EQL model for TiO_2 -aqueous solution interface

In pursuance of corroborating the flexible BL model for different solid-liquid interfaces, in this section, we develop an electrical quad-layer (EQL) model for the rutile (TiO_2)-aqueous solution interface. To this aim, the typical chemical reactions of the rutile surface adsorption can be written as [40]



where K_1^{int} , K_2^{int} , $K_{M^+}^{int}$, $K_{A^-}^{int}$ denote the equilibrium constants for the chemical reactions and define as

$$K_1^{int} = \frac{\sigma_{TiOH}}{\sigma_{TiOH_2^+}} n_{b,H^+} \exp(-\psi_0), \quad (24)$$

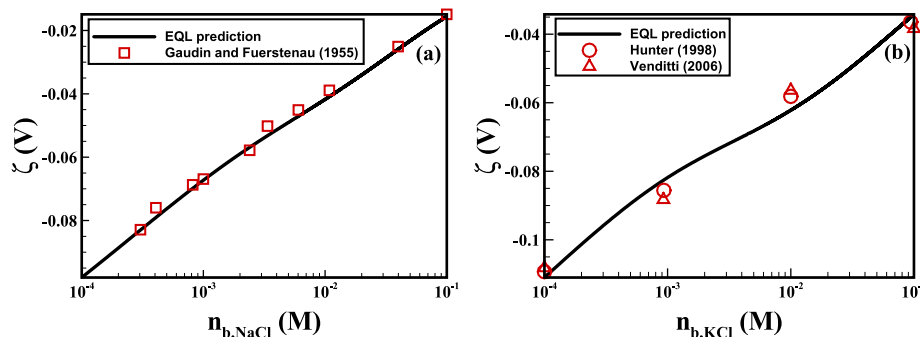


Fig. 3. The zeta potential for the SiO_2 -aqueous solution as a function of bulk ion concentration for (a) *NaCl* solution with pH = 6.5 and (b) *KCl* solution with pH = 7. The symbols are the experimentally measured zeta potential and the solid lines the predicted zeta potential with the proposed EQL model.

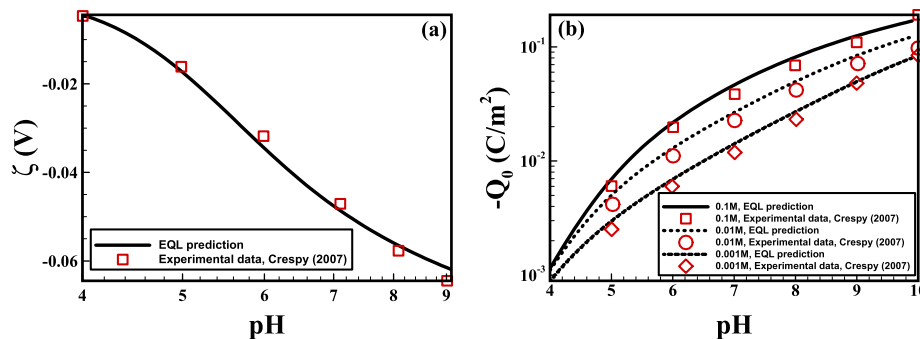


Fig. 4. The (a) zeta potential for 0.01 M *NaCl* concentration and (b) surface charge for SiO_2 -aqueous solution as a function of solution pH. The symbols are the experimentally measured zeta potential and the solid lines the predicted zeta potential with the proposed EQL model.

$$K_2^{int} = \frac{\sigma_{TiO^-}}{\sigma_{TiOH}} n_{b,H^+} \exp(-\bar{\psi}_0), \quad (25)$$

$$K_{M^+}^{int} = \frac{\sigma_{TiOM}}{\sigma_{TiO^-}} \frac{1}{n_{b,M^+}} \exp(\bar{\psi}_{IHP}), \quad (26)$$

$$K_A^{int} = \frac{\sigma_{TiOH_2A}}{\sigma_{TiOH_2^+}} \frac{1}{n_{b,A^-}} \exp(-\bar{\psi}_{IHP}), \quad (27)$$

where the equilibrium parameters are $K_2^{int} = 10^{-9.7}$, $K_A^{int}(pH) = Sgn[4 - pH]H[4 - pH] \times 10^3 + H[pH - 4] \times 10^{(3+0.33 \times (pH-4))}$ and $H[.]$ denotes the Heaviside step function and $Sgn[.]$ is the sign function [40]. Since the pH_{PZC} (pH of the point of zero charge) for rutile is around 6.1 [41], therefore, one can obtain $K_1^{int} = 10^{(-2pH_{PZC} - \log(K_2^{int}))}$. Considering the cation (M^+) adsorption to the rutile-aqueous solution interface, as we mentioned above, since we are focusing on the $pH < pH_{PZC}$, due to the high protonation reaction, the chemical reaction of Eq. (22) could be ignored ($\sigma_{TiOM} \approx 0$). Similar to the equations were mentioned for silica-aqueous solution interface in the previous section, we propose the following set of equations for the rutile as

$$e\Gamma^0 = \sigma_{TiOH} + \sigma_{TiO^-} + \sigma_{TiOH_2^+} + \sigma_{TiOH_2A}, \quad (28)$$

$$Q_0 = \sigma_{TiOH_2^+} - \sigma_{TiO^-} + \sigma_{TiOH_2A}, \quad (29)$$

$$Q_{IHP} = \sigma_{TiOH_2A}, \quad (30)$$

$$Q_{OHP} = -\sqrt{8\epsilon_0\epsilon_r k_B T n_{s,b}} \sinh(0.5\bar{\psi}_{OHP}) - Q_{ZP}, \quad (31)$$

$$Q_{ZP} = -\sqrt{8\epsilon_0\epsilon_r k_B T n_{s,b}} \sinh(0.5\bar{\psi}_{ZP}), \quad (32)$$

$$Q_0 + Q_{IHP} + Q_{OHP} + Q_{ZP} = 0, \quad (33)$$

$$\bar{\psi}_0 - \bar{\psi}_{IHP} = \frac{Q_0}{C_{IHP}}, \quad (34)$$

$$\bar{\psi}_{IHP} - \bar{\psi}_{OHP} = -\frac{Q_{OHP}}{C_{OHP}}, \quad (35)$$

$$\bar{\psi}_{OHP} - \bar{\psi}_{ZP} = -\frac{Q_{ZP}}{C_{BL}}. \quad (36)$$

By employing the Newton's method to solve the nonlinear system of equations, one can solve the set of Eqs. (24), (25), (27), (28–36) to obtain the unknown parameters of the EQL model for rutile-aqueous solution interface. We should note that for rutile, the sur-

face site density is $\Gamma^0 = 5.6 \text{ (nm}^{-1}\text{)}$ [42]. Considering the capacitance of the IHP and OHP, since the aqueous solution under consideration is the same and, on the other hand, the surface site density of SiO_2 and TiO_2 are approximately equal, consequently, we assumed the same capacitance for IHP and OHP with what was mentioned for the silica (Table 1). However, the differential capacitance of the BL should be determined based on the thickness of the BL for TiO_2 -aqueous solution interface. Fig. 5 demonstrates the results of our rutile FLM versus solution pH for NaCl . Our modeling results (Fig. 5a) show well agreement with the available experimental measurements of zeta potential [41] for two bulk ion concentrations 0.02 (M) and 0.2 (M). It is worthwhile to note that in Fig. 5a, the modeling results of molecular dynamics (MD) simulation (dash lines with symbols) also presented for bulk ion concentration 0 (M) and 0.41 (M) [29]. In order to obtain the best-fitted zeta potential with the experimental data, the thickness of the BL should be $\delta_{BL}^{0.02M} = 7 \text{ (nm)}$ and $\delta_{BL}^{0.2M} = 2.6 \text{ (nm)}$. This proves the flexibility of the BL as a function of bulk ion concentration for rutile-aqueous solution interface which resembles a reciprocal relation between δ_{BL} and the bulk ion concentration. Moreover, the rutile EQL model predicts the surface charge (Q_0) versus solution bulk ion concentration and pH (Fig. 5b). It is shown that for TiO_2 -aqueous solution interface, in general, by increasing the solution pH, the acquired surface charge decreases. However, for dilute solutions (0.001 M), the surface charge tends to zero for $pH > 5.5$.

Considering what we have found for SiO_2 - and TiO_2 -aqueous solution interface, it is elucidated that the ion transport mechanism lies in by increasing the bulk ion concentration, wider area of the charged nanochannels or nanopores would be electrokinetically active and contribute to electrokinetic transport. It is noteworthy that the proposed EQL model for SiO_2 and TiO_2 could be simply modified to obtain the surface charge and zeta potential for higher valence symmetric and asymmetric solutions (i.e. CaCl_2).

3. Results and discussion

3.1. Helmholtz free energy of the buffer layer

We intend to figure out the Helmholtz free energy ($F = U_{ele} - TS$) of BL and DL by employing Eq. (A.2) and (A.3), and the available analytical solution [43] the electrical potential $\bar{\psi} = 2\ln\left(\left(1 + \exp(-\kappa x)\tanh(\bar{\psi}_{OHP}/4)\right)\left(1 - \exp(-\kappa x)\tanh(\bar{\psi}_{OHP}/4)\right)^{-1}\right)$ where $\bar{\psi}_{OHP}$ is obtained by solving our proposed EQL model for SiO_2 (Section 2.1.1). Fig. 6 shows the Helmholtz free energy as a function of distance from the OHP for different bulk ion concentration of KCl

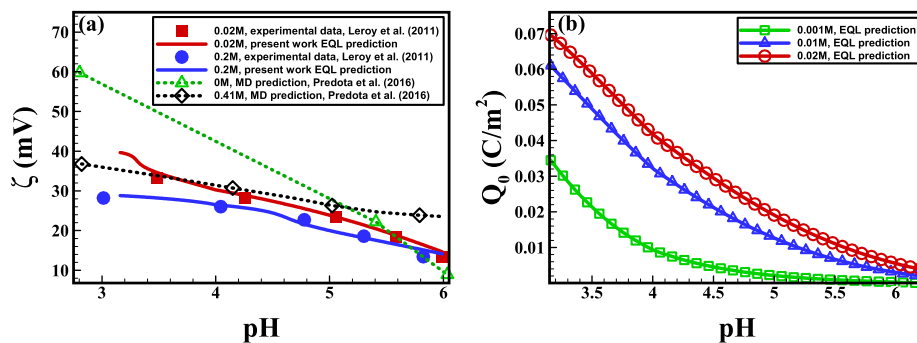


Fig. 5. The (a) zeta potential and (b) surface charge for rutile TiO_2 -aqueous solution as a function of solution pH and NaCl concentration at $T = 25 \text{ }^\circ\text{C}$. Our proposed EQL model for the rutile-aqueous interface predicted well agreement zeta potentials with the available experimental measurements [41] for a NaCl solution with a concentration of 0.02 (M) and 0.2 (M). The molecular dynamics (MD) simulations of the Predota et al. [29] are presented for a solution with 0 (M) and 0.41 (M) bulk ion concentration.

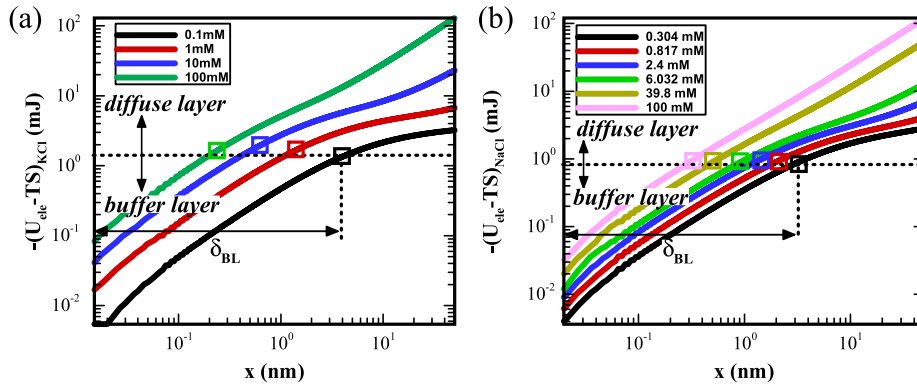


Fig. 6. The Helmholtz free energy ($F = U_{ele} - TS$) of the solution as a function of distance (x) from the OHP for (a) KCl and (b) $NaCl$ solutions. The colorful square symbols represent the thickness of the BL (δ_{BL}) for each bulk ion concentration which obtained by our EQL model. Our modeling results show that for both KCl and $NaCl$ solutions, the Helmholtz free energy of the buffer layer is independent of the bulk ion concentration while changes for different solutions as $F_{BL,KCl} > F_{BL,NaCl}$.

and $NaCl$ solutions. If we mark off the corresponding amount of $-F$ at $x = \delta_{BL}$ for different bulk ion concentration (the colorful square symbols in Fig. 6a and b), interestingly we found that the Helmholtz free energy of BL (for constant pressure and temperature) is independent of bulk ion concentration ($\partial F_{BL}/\partial n_{M,b} \approx 0$), whereas it changes for different solutions. As a matter of fact, the Helmholtz free energy in the electric double layer is determined by the competition of self-energy of the electric field and the ion's energy within this field. Thus, although for a lower amount of bulk ion concentration we have stronger self-energy of the electric field, however, the energy of the ions is smaller compared with the higher bulk ion concentration. Results in Fig. 6 support this interpretation that for a certain x , the free energy ($-F$) increases with bulk ion concentration.

3.2. Ionic conductance of nanochannels

Employing the proposed theory of the flexible BL (FBL) model with direct numerical solution of PNP model [6] to obtain the ionic conductance of narrow nanochannels explains the main reason underlying of why a 2 nm-height nanochannel with negatively charged walls has conductance on the order of deionized (DI) water [31] for low ionic strengths. Recalling the results for the thickness of BL (Fig. 2b), we define the effective height of the nanochannel as $H_{eff} = H - 2(\delta_{BL} + \delta_{IHP} + \delta_{OHP})$. We obtain the ionic conductance ($G = I/E$) of the nanochannel by calculating the ionic current through the nanochannel as

$$I = w \int_{-H_{eff}/2}^{H_{eff}/2} \left\{ u(x,y) \rho_e(x,y) - \tilde{D} \nabla (\rho_e(x,y)) - \tilde{D} \nabla (\bar{\psi}(x,y) + \bar{\phi}(x,y)) \right. \\ \left. \times \sum e z_i^2 n_i(x,y) \right\} dy \quad (37)$$

where $w = 2 \mu\text{m}$ H , u and $\rho_e = e \sum z_i n_i$ denote the width of nanochannel, the height of nanochannel, the fluid flow velocity, and the net electric charge density, respectively. In this equation, $\tilde{D} = (D_{K^+} + D_{Cl^-})/2$, $\bar{\psi} = \psi/V_T$, $\bar{\phi} = \psi/V_T$, and n_i are the averaged diffusion coefficient, the dimensionless electric potential, the dimensionless applied electric potential, and the distribution of the co- and counter-ions, respectively. Here, $V_T = k_B T/e$ represents the thermal voltage. To obtain the ionic current, we need to solve the Poisson-Nernst-Planck and Navier-Stokes equations coupled with the non-linear set of EQL model equations. Fig. 7a shows that the EQL model coupled with PNP equations [6] predicts ionic conductance in nanochannels with good agreements with what has been measured by Duan and Majumdar [31].

We have to note that the proposed EQL model has been developed for a chemically-isolated solid-liquid interface. For chemically non-isolated interfaces (i.e. narrow nanochannel with overlapped EDLs) we have employed an enrichment coefficient [6] which is introduced to the EQL model to take into account the interactions of EDLs in narrow nanochannels. Here we point out that for low bulk ion concentration where $H_{eff} < 0$, the EQL model predicts that the whole nanochannel is covered by SL and BL. However, by increasing the bulk ion concentration, the ZP approaches toward the solid surface where the thickness of SL + BL will be smaller than half of the nanochannel height and eventually to ionic conductance beyond the DI water. To investigate the influence of bulk ion concentration and nanochannel height on electrical conductance, we employ the EQL model with PNP equations to obtain ionic conductance of electrokinetically active area of narrow nanochannels. Fig. 7b shows the contour of the electrical conductance with contour lines of isoelectrical ionic conductance. Our modeling results illustrate that the ionic conductance remains

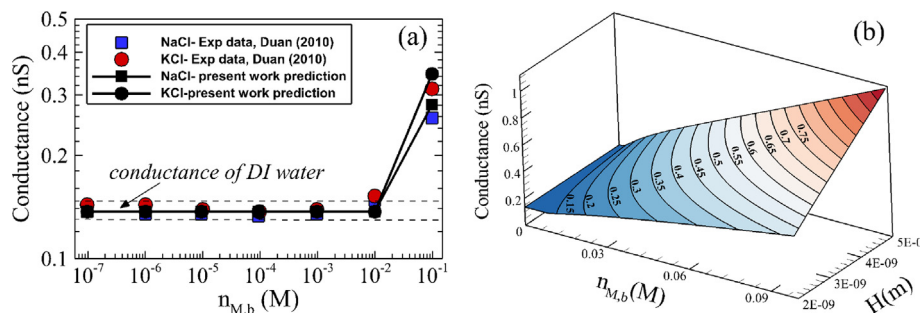


Fig. 7. (a) The experimental data [31] and present work modeling results for electrical conductance of ten parallel 2 nm nanochannels versus bulk ion concentration. The experimental results predicted the conductance of deionized (DI) water for $n_{M,b} < 10^{-2}$ (M). (b) Modeling results of nanochannel conductance versus bulk ion concentrations and nanochannel heights. The contour lines demonstrate the isoelectrical conductance values.

unchanged by increasing the height of nanochannel and decreasing the bulk ion concentration (moving on contour lines). The main reason in favor of this fact is, though, the height of nanochannel is increasing, the thickness of the BL also increasing (due to decreasing of bulk ion concentration) which reduces the ionic conductance enhancement owing to the nanochannel height increment. In other word, Fig. 7b implies the fact that in order to attain a certain amount of nanochannel conductance, there are minimum and maximum values for both nanochannel height and bulk ion concentration.

4. Conclusions

We have shown that the position of zeta potential plane is a function of the bulk ionic concentration. A new layer, so-called buffer layer, is introduced between the zeta potential plane and the outer-Helmholtz layer in order to propose a near-to-reality model to predict the acquired surface charge for different solid-liquid interfaces. Two interesting characteristic features of this layer have been unveiled by varying the bulk ion concentration: (i) the flexible thickness and (ii) the invariant Helmholtz free energy. The flexibility of the buffer layer is corroborated not only by thermodynamic analysis but also by comparisons with the measured zeta potential for silica (SiO₂)- and rutile (TiO₂)-aqueous solution interfaces. It has been found that the underneath of zeta potential plane has shrunk by increasing the bulk ion concentration. This phenomenon is similar to the well-understood behavior of diffuse layer (electrokinetically active part of EDL) which characterized by the Debye length. Employing the proposed model for ion transport through narrow nanochannel has revealed the transport mechanism in such a confined space. Good agreements of our predictions with the experimental measurements of ionic conductance elucidated a substantial fact that the electrokinetically active area of charged nanochannels or nanopores varies as a function of bulk ion concentration.

Acknowledgment

This work was financially supported by the NSF grant of China (No. 51676107). The authors would also like to thank Dr. Derek Stein, Dr. Chuanhua Duan, Dr. Andre Revil, Dr. Milan Predota, Dr. Itamar Borukhov, and Dr. Hirofumi Daiguji for fruitful discussions.

Appendix A. Thermodynamic analysis for flexibility of the buffer layer

In order to investigate the properties of the introduced BL, we performed a thermodynamic analysis. Since the DL and Stern layer (SL) exchange ions through BL, one can consider these two layers as two systems in contact. In thermodynamic equilibrium state in which the total differential Gibbs free energy ($G = U_{ele} + pV - TS$, where U_{ele} denotes the electrostatic energy, V the volume of the system, and TS the entropic energy) of these isobar and isotherm systems is [38]

$$dG = \sum_i \mu_i dN_i = \sum_i (\mu_{i,BL+SL} dN_{i,BL+SL} + \mu_{i,DL} dN_{i,DL}) = 0, \quad (A.1)$$

where G (J) and N_i (mol) denote the Gibbs free energy and the i th ion concentration, respectively, the ion conservation principle ($dN_{i,BL+SL} = -dN_{i,DL}$) imposes the equality of $\mu_{i,BL+SL}$ (J mol⁻¹) electrochemical potential of SL + BL and DL ($\mu_{i,BL+SL} = \mu_{i,DL}$) denotes the representative electrochemical potential of the i th ion for BL and SL. Accordingly, for a system at constant pressure (p) and temperature (T) we have

$$\mu_{i,BL+SL} = \mu_{i,DL} \rightarrow \left(\frac{\partial G}{\partial n_{b,i}} \right)_{T,p}^{BL+SL} = \left(\frac{\partial G}{\partial n_{b,i}} \right)_{T,p}^{DL}, \quad (A.2)$$

where $\bar{n}_{b,i}$ (mol) is the bulk i th ion concentration. By employing the mean-field theory, the electrostatic energy in terms of the local ion concentration c^\pm (m⁻³) and electrostatic potential $\psi(V)$ for a 1:1 ionic system is [44,45]

$$U_{ele} = A \int \left(\frac{-\epsilon_0 \epsilon_r |\nabla \psi(\mathbf{x})|^2}{2} + zec^+(\mathbf{x})\psi(\mathbf{x}) - zec^-(\mathbf{x})\psi(\mathbf{x}) \right) dx, \quad (A.3)$$

where A (m²), $\epsilon_0 \epsilon_r$ (CV⁻¹ m⁻¹), and N_A (mol⁻¹) denote the area of the solid surface, the electrical permittivity of the solution, and Avogadro number, respectively. The first term at the right-hand side of Eq. (A.3) is the self-energy of the electric field which could be written in terms of the electro-viscosity as $-\epsilon_0 \epsilon_r (\bar{\eta} - 1)/2f$, where f (V⁻² m²) is the viscoelectric coefficient [46] and $\bar{\eta} \equiv \eta_e/\eta_0 = (1 + f(d\psi/dx)^2)$ denotes the normalized electroviscosity with the solution viscosity. The next two terms demonstrate the electrostatic energy of the ions within the local electric field. Regarding the entropic contribution in Gibbs free energy, we have [45]

$$-TS = Ak_B T \int (c^+(\mathbf{x}) \ln(c^+(\mathbf{x})\vartheta) + c^-(\mathbf{x}) \ln(c^-(\mathbf{x})\vartheta)) dx, \quad (A.4)$$

where $k_B T$ is the thermal energy and $\vartheta = (4/3)\pi r^3$ the volume of the ion where r (m) denotes the radius of the ion. For sake of simplicity, we assume that the bulk ion concentration is high enough ($\kappa H \gg 1$) which results in $\bar{\psi} \equiv \psi/V_T \ll 1$, where κ (m⁻¹) = $\sqrt{2e^2 n_b / \epsilon_0 \epsilon_r k_B T}$ and $V_T(V) = k_B T/e$ denote the reverse of the Debye length and thermal voltage, respectively. In Debye length, n_b (m⁻³) is the number density of the ions. By considering a linear local electric potential as a function of distance from the solid surface for SL $\psi(\mathbf{x})|_0^{X_{OHP}} = ((\psi_{OHP} - \psi_0)/X_{OHP})x + \psi_0$ and exponentially decaying function for BL and DL as $\psi(\mathbf{x})|_{X_{OHP}}^{X_{ZP}} = \psi_{OHP} \exp(-\kappa(x - X_{OHP}))$, $\psi(\mathbf{x})|_{X_{ZP}}^{X_{DL}} = \psi_{ZP} \exp(-\kappa(x - X_{ZP}))$, (we employ the Boltzmann ion distribution $c^\pm = n_b \exp(\mp \bar{\psi})$ for simplicity), and introducing Eqs. (A.3) and (A.4) into Eq. (A.2), finally we have

$$\left(p_\infty \frac{\partial V}{\partial n_b} \right)_{SL+BL} = \left(\frac{\partial U_{ele}}{\partial n_b} + p_\infty \frac{\partial V}{\partial n_b} - T \frac{\partial S}{\partial n_b} \right)_{DL} - \left(\frac{\partial U_{ele}}{\partial n_b} - T \frac{\partial S}{\partial n_b} \right)_{SL+BL}. \quad (A.5)$$

In Eq. (A.5) (Appendix B)

$$\left(-T \frac{\partial S}{\partial n_b} \right)_{DL} + \left(T \frac{\partial S}{\partial n_b} \right)_{SL+BL} \approx Ak_B T \left(F(\bar{\psi}(X_{ZP}), \delta_{DL}) - F(\bar{\psi}(X_{OHP}), \delta_{BL}) - X_{OHP} (2 + \ln(n_b \vartheta)) \right), \quad (A.6)$$

where $F(\bar{\psi}(X_{ZP}), \delta_{DL}) = \delta_{DL} \exp(-\bar{\psi}_{ZP}) (\ln(-\bar{\psi}_{ZP} n_b \vartheta) + 1)$ and $F(\bar{\psi}(X_{OHP}), \delta_{BL}) = \delta_{BL} \exp(-\bar{\psi}_{OHP}) (\ln(-\bar{\psi}_{OHP} n_b \vartheta) + 1)$ denote functions which return a distance. This function is assumed as a mathematical shortcut for easy demonstration of the variation of entropic contribution with respect to bulk ion concentration. For concentrated solutions, it can be shown that $2 + \ln(n_b \vartheta) > 0$ and $F(\bar{\psi}(X_{ZP}), \delta_{DL}) - F(\bar{\psi}(X_{OHP}), \delta_{BL}) < 0$ which eventuates to the higher variation of entropic energy (TS) with respect to bulk ion concentration for DL compared with SL + BL. In other words, Eq. (A.6) states that the entropic energy of DL increases more compared with the

entropic energy of the SL + BL when the bulk ion concentration increases. Considering the electrostatic energy, we have (Appendix B)

$$\left(\frac{\partial U_{ele}}{\partial n_b}\right)_{DL} - \left(\frac{\partial U_{ele}}{\partial n_b}\right)_{SL+BL} \approx \frac{\varepsilon_0 \varepsilon_r}{2f} \left(\frac{(\bar{\eta}_{ave} - 1) \partial V_{SL+BL}}{\partial n_b} + \frac{V_{SL+BL} \partial(\bar{\eta}_{ave})}{\partial n_b} \right), \quad (\text{A.7})$$

where $\bar{\eta}_{ave}$ defines the mean electro-viscosity within the SL + BL as $\bar{\eta}_{ave} = \int_0^{X_{ZP}} \bar{\eta} dx / X_{ZP}$, where X_{ZP} denotes the distance of ZP from a solid surface (Fig. 1). In Eq. (A.7), the first term in the right-hand side represents the variations of the volume of SL + BL due to the electro-viscosity. The second term represents the variation of mean electro-viscosity with respect to the bulk ion concentration, which is negative because the electro-viscosity decreases with an increasing bulk ion concentration. In Eq. (A.5), the derivative of the volume of DL ($V_{DL} = \kappa^{-1}A$) with respect to the bulk ion concentration is $(-0.5A p_\infty \sqrt{\varepsilon_0 \varepsilon_r k_B T / 2e^2 n_b}) n_b^{-1}$ which is negative for all n_b . Eventually, from Eq. (A.5), it is deduced that the total volume of the SL + BL decreases by increasing the bulk ion concentration ($\partial V_{SL+BL} / \partial n_b < 0$). This relation unveils a substantial fact that, from a thermodynamic viewpoint, the thickness of BL and, subsequently, the position of zeta potential plane behaves flexible in response to the bulk ion concentration (Fig. 2a).

Appendix B. Mathematical operations for thermodynamic analysis

B.1. Derivative of electrostatic energy with respect to n_b for SL + BL and DL

Considering the first term on the right-hand side of Eq. (A.3) which represents the self-energy of the electric field, one can redefine this term based on the electro-viscosity as $-\varepsilon_0 \varepsilon_r (\bar{\eta} - 1) / 2f$ where $\bar{\eta} = \eta_e / \eta_0$ and $\eta_e = \eta_0 (1 + f(d\psi/dx)^2)$. As a result, Eq. (A.3) could be written in terms of the electro-viscosity as

$$U_{ele}|_{SL+BL} = A \int \left(\frac{-\varepsilon_0 \varepsilon_r (\bar{\eta} - 1)}{2f} + zec^+(\mathbf{x})\psi(\mathbf{x}) \right) dx, \quad (\text{B.1})$$

and for DL we have

$$U_{ele}|_{DL} = A \int (zec^+(\mathbf{x})\psi(\mathbf{x})) dx. \quad (\text{B.2})$$

Herein for simplicity, we ignore the effects of the co-ions c^- on the electrostatic energy. By introducing $\psi(x)|_0^{X_{OHP}} = ((\psi_{OHP} - \psi_0) / X_{OHP})x + \psi_0$, $\psi(x)|_{X_{OHP}}^{X_{ZP}} = \psi_{OHP} \exp(-\kappa(x - X_{OHP}))$, and $\psi(x)|_{X_{ZP}}^{X_{DL}} = \psi_{ZP} \exp(-\kappa(x - X_{ZP}))$ to Eq. (B.1) one can obtain the electrostatic internal energy for SL + BL as

$$U_{ele}|_{SL+BL} = A \int_0^{X_{ZP}} \left(\frac{-\varepsilon_0 \varepsilon_r (\bar{\eta} - 1)}{2f} \right) dx + A \int_0^{X_{OHP}} (zen_b \exp(-\bar{\psi}_{0-X_{OHP}}(x)) (\psi_{0-X_{OHP}}(x))) dx + A \int_{X_{OHP}}^{X_{ZP}} (zen_b \exp(-\bar{\psi}_{OHP} \exp(-\kappa(x - X_{OHP}))) (\psi_{OHP} \exp(-\kappa(x - X_{OHP})))) dx, \quad (\text{B.3})$$

where $\bar{\psi}_{0-X_{OHP}}(x) = \frac{\bar{\psi}_{OHP} - \bar{\psi}_0}{X_{OHP}} x + \bar{\psi}_0$ and $0 < x < X_{OHP}$. Here we should note that $\bar{\psi} = \psi / v_T$ where $v_T = k_B T / e$ denotes the thermal voltage.

Considering the first term on the right-hand side of Eq. (B.3), we simplify this term by averaging of the electro-viscosity along the SL + BL as

$$\int_0^{X_{ZP}} \left(\frac{-\varepsilon_0 \varepsilon_r (\bar{\eta} - 1)}{2f} \right) dx = \frac{-\varepsilon_0 \varepsilon_r X_{ZP}}{2f} (\bar{\eta}_{ave} - 1), \quad (\text{B.4})$$

where $\bar{\eta}_{ave} = \int_0^{X_{ZP}} \bar{\eta} dx / X_{ZP}$. For the second term which is responsible for the electrostatic energy of the SL, one can simply integrate and has

$$\int_0^{X_{OHP}} (\exp(\bar{\psi}_{0-X_{OHP}}(x)) (\psi_{0-X_{OHP}}(x))) dx = -v_T X_{OHP} \exp(-\bar{\psi}_{OHP}) - v_T X_{OHP} \left(\frac{\bar{\psi}_0 + 1}{\bar{\psi}_{OHP} - \bar{\psi}_0} \right) (\exp(-\bar{\psi}_{OHP}) - \exp(-\bar{\psi}_0)). \quad (\text{B.5})$$

For the second term on the right-hand side of Eq. (B.3) which deals with the electrostatic energy of the BL, we have

$$\int_{X_{OHP}}^{X_{ZP}} (\exp(-\bar{\psi}_{OHP} \exp(-\kappa(x - X_{OHP}))) (\psi_{OHP} \exp(-\kappa(x - X_{OHP})))) dx = v_T \kappa^{-1} (\exp(-\bar{\psi}_{OHP} \exp(-\kappa(X_{ZP} - X_{OHP}))) - \exp(-\bar{\psi}_{OHP})), \quad (\text{B.6})$$

where $\kappa(\text{m}^{-1}) = \sqrt{2e^2 n_b / \varepsilon_0 \varepsilon_r k_B T}$ denotes the reverse of the Debye length as the characteristic length of the DL. By introducing Eqs. (B.4) to (B.6) into Eq. (B.3) one has the total electrostatic energy of the SL + BL as

$$U_{ele}|_{SL+BL} = \frac{-\varepsilon_0 \varepsilon_r (V_{SL} + V_{BL})}{2f} (\bar{\eta}_{ave} - 1) + z e v_T n_b \left(V_{SL} \left(-\exp(-\bar{\psi}_{OHP}) - \left(\frac{\bar{\psi}_0 + 1}{\bar{\psi}_{OHP} - \bar{\psi}_0} \right) (\exp(-\bar{\psi}_{OHP}) - \exp(-\bar{\psi}_0)) \right) + A \kappa^{-1} (\exp(-\bar{\psi}_{OHP} \exp(-\kappa(X_{ZP} - X_{OHP}))) - \exp(-\bar{\psi}_{OHP})) \right), \quad (\text{B.7})$$

where $V_{SL} = A X_{OHP}$ represents the volume of the SL.

On the other hand, the electrostatic energy of the DL would be as

$$U_{ele}|_{DL} = A \int_{X_{ZP}}^{X_{DL}} zec^+(\mathbf{x})\psi(\mathbf{x}) dx = A z e n_b v_T \kappa^{-1} (\exp(-\bar{\psi}_{ZP} \exp(-\kappa(X_{DL} - X_{ZP}))) - \exp(-\bar{\psi}_{ZP})). \quad (\text{B.8})$$

For simplifying the obtained electrostatic energy of the SL + BL and DL, we assume high bulk ion concentration ($\kappa H \gg 1$) and as a result $\bar{\psi} \ll 1$. If so, by employing the Taylor expansion, we have

$$\exp(-\bar{\psi}_{OHP}) - \exp(-\bar{\psi}_0) \approx \bar{\psi}_0 - \bar{\psi}_{OHP} \quad (\text{B.9})$$

Considering Eq. (B.8), we can simplify that as

$$U_{ele}|_{DL} \approx 0, \quad (\text{B.10})$$

By introducing Eq. (B.9) to Eq. (B.7) for SL + BL, we finally have

$$U_{ele}|_{SL+BL} \approx \frac{-\varepsilon_0 \varepsilon_r (V_{SL} + V_{BL})}{2f} (\bar{\eta}_{ave} - 1) + 2ze v_T n_b V_{SL} \bar{\psi}_0, \quad (\text{B.11})$$

where V_{SL} is a constant amount which is a function of the ionic size. Taking the partial derivative with respect to the bulk ion concentration from Eqs. (B.10) and (B.11), one has

$$\frac{\partial U_{ele}}{\partial n_b} \Big|_{SL+BL} \approx -\frac{\varepsilon_0 \varepsilon_r}{2f} \left(\frac{(\bar{\eta}_{ave} - 1) \partial V_{SL+BL}}{\partial n_b} + \frac{V_{SL+BL} \partial(\bar{\eta}_{ave})}{\partial n_b} \right) + 2ze v_T V_{SL} \bar{\psi}_0 \quad (\text{B.12})$$

$$\frac{\partial U_{ele}}{\partial n_b} \Big|_{DL} \approx 0 \quad (\text{B.13})$$

Considering the fact that $V_{SL}\bar{\psi}_0 \ll 1$ therefore we can ignore the second term on the right-hand side of Eq. (B.12) compared with the first term. So, the difference of the electrostatic energy of DL and SL + BL would be as

$$\left. \frac{\partial U_{ele}}{\partial n_b} \right|_{DL} - \left. \frac{\partial U_{ele}}{\partial n_b} \right|_{SL+BL} \approx \frac{\varepsilon_0 \varepsilon_r}{2f} \left(\frac{(\bar{n}_{ave} - 1) \partial V_{SL+BL}}{\partial n_b} + \frac{V_{SL+BL} \partial (\bar{n}_{ave})}{\partial n_b} \right) \quad (\text{B.14})$$

It would be interesting to note that the electrostatic energy of the diffuse layer does not change with the bulk ion concentration when we have high bulk ion concentration.

B.2. Derivative of entropic energy with respect to n_b for SL + BL and DL

Regarding the contribution of the entropic energy, for a solution at which the Steric effects could be ignored, we have [45]

$$-TS = Ak_B T \int (c^+(\mathbf{x}) \ln(c^+(\mathbf{x})\vartheta) + c^-(\mathbf{x}) \ln(c^-(\mathbf{x})\vartheta)) dx, \quad (\text{B.15})$$

where $k_B T$ is the thermal energy and $\vartheta = (4/3)\pi r^3$ denotes the volume of the ions. If we introduce $\psi(x)|_{X_{OHP}}^{X_{OHP}} = ((\psi_{OHP} - \psi_0)/X_{OHP})x + \psi_0$, $\psi(x)|_{X_{OHP}}^{X_{OHP}} = \psi_{OHP} \exp(-\kappa(x - X_{OHP}))$, and $\psi(x)|_{X_{OHP}}^{X_{OHP}} = \psi_{OHP} \exp(-\kappa(x - X_{OHP}))$ and $c^\pm = n_b \exp(\mp e\psi/k_B T)$ into Eq. (B.15), for the SL + BL and re-calling the thin electric double layer assumptions, one has

$$-TS|_{SL} \approx k_B T n_b V_{OHP} (\ln(n_b \vartheta) + 1). \quad (\text{B.16})$$

For the BL, we have

$$\begin{aligned} -TS|_{BL} \approx & Ak_B T n_b \exp(-\bar{\psi}_{OHP}) \left(\ln(-\bar{\psi}_{OHP} n_b \vartheta) (X_{ZP} - X_{OHP} + 0.5\kappa \bar{\psi}_{OHP} (X_{ZP} - X_{OHP})^2) \right. \\ & \left. - Ak_B T n_b \exp(-\bar{\psi}_{OHP}) \left(\kappa (0.5(X_{ZP} - X_{OHP})^2 + \frac{\kappa \bar{\psi}_{OHP}}{3} (X_{ZP} - X_{OHP})^3) \right) \right). \end{aligned} \quad (\text{B.17})$$

Eq. (B.17) could be obtained by introducing $\psi(x)|_{X_{OHP}}^{X_{ZP}} = \psi_{OHP} \exp(-\kappa(x - X_{OHP}))$ and $c^\pm = n_b \exp(\mp e\psi/k_B T)$ into Eq. (A.4) where by employing the Taylor expansion around the $x = X_{OHP}$ we have (based on the assumption of $\bar{\psi}_{OHP} \ll 1$)

$$\begin{aligned} & \exp(-\bar{\psi}_{OHP} \exp(-\kappa(x - X_{OHP}))) \\ & \approx \exp(-\bar{\psi}_{OHP}) \left(1 + \kappa \bar{\psi}_{OHP} (x - X_{OHP}) \right). \end{aligned} \quad (\text{B.18})$$

By the aid of this expansion, we could simply take the integral from Eq. (A.4) for BL. Considering Eq. (B.17), we can ignore the terms $0.5\kappa \bar{\psi}_{OHP} (X_{ZP} - X_{OHP})^2$ and $\kappa \bar{\psi}_{OHP} (X_{ZP} - X_{OHP})^3/3$ since $\bar{\psi}_{OHP} \kappa (X_{ZP} - X_{OHP}) \ll 1$ and $\bar{\psi}_{OHP} \kappa (X_{ZP} - X_{OHP})^2/3 \ll 1$. As a result, Eq. (B.17) could be re-written as

$$-TS|_{BL} \approx Ak_B T n_b \exp(-\bar{\psi}_{OHP}) \left(\ln(-\bar{\psi}_{OHP} n_b \vartheta) (X_{ZP} - X_{OHP}) - 0.5\kappa (X_{ZP} - X_{OHP})^2 \right). \quad (\text{B.19})$$

Similarly, we can obtain the entropic energy for DL as

$$-TS|_{DL} \approx Ak_B T n_b \exp(-\bar{\psi}_{ZP}) \left(\ln(-\bar{\psi}_{ZP} n_b \vartheta) (X_{DL} - X_{ZP}) - 0.5\kappa (X_{DL} - X_{ZP})^2 \right). \quad (\text{B.20})$$

Taking the partial derivative with respect to bulk ion concentration ($-T \partial S / \partial n_b$) for both SL + BL and DL gives rise to

$$\begin{aligned} & \left(-T \frac{\partial S}{\partial n_b^+} \right)_{DL} + \left(T \frac{\partial S}{\partial n_b^+} \right)_{SL+BL} \approx Ak_B T \left(F(\bar{\psi}(X_{ZP}), \delta_{DL}) \right. \\ & \left. - F(\bar{\psi}(X_{OHP}), \delta_{BL}) - X_{OHP} (2 + \ln(n_b \vartheta)) \right), \end{aligned} \quad (\text{B.21})$$

where $F(\bar{\psi}(X_{ZP}), \delta_{DL}) = \delta_{DL} \exp(-\bar{\psi}_{ZP}) \left(\ln(-\bar{\psi}_{ZP} n_b \vartheta) + 1 \right)$ and $F(\bar{\psi}(X_{OHP}), \delta_{BL}) = \delta_{BL} \exp(-\bar{\psi}_{OHP}) \left(\ln(-\bar{\psi}_{OHP} n_b \vartheta) + 1 \right)$ denote functions which return a distance. It is assumed as a mathematical shortcut for easy demonstration of the variation of entropic contribution with respect to bulk ion concentration. It should be noted that for Eq. (B.21) we neglect some terms with smaller order during the partial derivative process.

Appendix C. Supplementary material

Supplementary data associated with this article can be found, in the online version, at <https://doi.org/10.1016/j.jcis.2018.09.010>.

References

- [1] B. Hille, *Ion Channels of Excitable Membranes*, third ed., Sinauer, Sunderland, MA, 2001.
- [2] H. Daiguji, P.D. Yang, A. Majumdar, Ion transport in nanofluidic channels, *Nano Lett.* 4 (2004) 137–142.
- [3] R. Karnik, C. Duan, K. Castelino, H. Daiguji, A. Majumdar, Rectification of ionic current in a nanofluidic diode, *Nano Lett.* 7 (2007) 547–551.
- [4] D. Stein, M. Kruthof, C. Dekker, Surface-charge-governed ion transport in nanofluidic channels, *Phys. Rev. Lett.* 93 (2004) 4.
- [5] F.H.J. van der Heyden, D. Stein, C. Dekker, Streaming currents in a single nanofluidic channel, *Phys. Rev. Lett.* 95 (2005) 4.
- [6] A. Alizadeh, M.E. Warkiani, M. Wang, Manipulating electrokinetic conductance of nanofluidic channel by varying inlet pH of solution, *Microfluid. Nanofluid.* 21 (2017) 52.
- [7] H. Daiguji, Y. Oka, K. Shirono, Nanofluidic diode and bipolar transistor, *Nano Lett.* 5 (2005) 2274–2280.
- [8] J. Hwang, H. Daiguji, Ion transport in Sub-10 nm nanofluidic channels: synthesis measurement and modeling, *Israel J. Chem.* 54 (2014) 1509–1518.
- [9] F.H.J. van der Heyden, D.J. Bonthuis, D. Stein, C. Meyer, C. Dekker, Electrokinetic energy conversion efficiency in nanofluidic channels, *Nano Lett.* 6 (2006) 2232–2237.
- [10] F.H.J. van der Heyden, D.J. Bonthuis, D. Stein, C. Meyer, C. Dekker, Power generation by pressure-driven transport of ions in nanofluidic channels, *Nano Lett.* 7 (2007) 1022–1025.
- [11] C. Zhong, Y. Deng, A.F. Roudsari, A. Kapetanovic, M.P. Anantram, M. Rolandi, A polysaccharide bioprotonic field-effect transistor, *Nat. Commun.* 2 (2011) 476.
- [12] K. Tybrandt, R. Forchheimer, M. Berggren, Logic gates based on ion transistors, *Nat. Commun.* 3 (2012) 871.
- [13] W. Guan, R. Fan, M.A. Reed, Field-effect reconfigurable nanofluidic ionic diodes, *Nat. Commun.* 2 (2011) 506.
- [14] J. Maier, Nanoionics: ion transport and electrochemical storage in confined systems, *Nat. Mater.* 4 (2005) 805.
- [15] M. Tagliazucchi, I. Szleifer, Salt pumping by voltage-gated nanochannels, *J. Phys. Chem. Lett.* 6 (2015) 3534–3539.
- [16] Y. Qiu, R.A. Lucas, Z.S. Siwy, Viscosity and conductivity tunable diode-like behavior for meso- and micropores, *J. Phys. Chem. Lett.* 8 (2017) 3846–3852.
- [17] W. Li, Y. Yan, M. Wang, P. Král, C. Dai, J. Zhang, Correlated rectification transport in ultranarrow charged nanocones, *J. Phys. Chem. Lett.* 8 (2017) 435–439.
- [18] A. Revil, P.A. Pezard, P.W.J. Glover, Streaming potential in porous media 1. Theory of the zeta potential, *J. Geophys. Res.-Solid Earth* 104 (1999) 20021–20031.
- [19] R.F. Probstein, *Physicochemical Hydrodynamics, and Introduction*, second ed., Wiley interscience, New York, 2003.
- [20] W.-L. Hsu, H. Daiguji, D.E. Dunstan, M.R. Davidson, D.J.E. Harvie, Electrokinetics of the silica and aqueous electrolyte solution interface: Viscoelectric effects, *Adv. Colloid Interface Sci.* 234 (2016) 108–131.
- [21] R.J. Hunter, *Zeta Potential in Colloid Science: Principles and Applications*, third ed., Academic Press, New York, 1988. DOI.
- [22] J. Lyklema, S. Rovillard, J. De Coninck, Electrokinetics: the properties of the stagnant layer unraveled, *Langmuir* 14 (1998) 5659–5663.
- [23] W.G. Eversole, W.W. Boardman, The effect of electrostatic forces on electrokinetic potentials, *J. Chem. Phys.* 9 (1941) 798–801.
- [24] W.G. Eversole, P.H. Lahr, Evidence for a rigid multilayer at a solid-liquid interface, *J. Chem. Phys.* 9 (1941) 530–534.
- [25] J.J. Bikerman, Immobile layer at the solid-liquid interface, *J. Chem. Phys.* 9 (1941) 880.
- [26] J. Lyklema, J.T.G. Overbeek, On the interpretation of electrokinetic potentials, *J. Colloid Sci.* 16 (1961) 501–512.
- [27] A.J. McMullen, J.X. Tang, D. Stein, Nanopore measurements of filamentous viruses reveal a sub-nanometer-scale stagnant fluid layer, *ACS Nano* 11 (2017) 11669–11677.
- [28] J. Lyklema, Molecular interpretation of electrokinetic potentials, *Curr. Opin. Colloid Interface Sci.* 15 (2010) 125–130.

- [29] M. Predota, M.L. Machesky, D.J. Wesolowski, Molecular origins of the zeta potential, *Langmuir* 32 (2016) 10189–10198.
- [30] J. Lyklema, Surface charges and electrokinetic charges: distinctions and juxtapositionings, *Colloids Surf. A* 376 (2011) 2–8.
- [31] C. Duan, A. Majumdar, Anomalous ion transport in 2-nm hydrophilic nanochannels, *Nat. Nanotechnol.* 5 (2010) 848–852.
- [32] H. Daiguji, High mobility in tight spaces, *Nat. Nanotechnol.* 5 (2010) 831.
- [33] A. Kitamura, K. Fujiwara, T. Yamamoto, S. Nishikawa, H. Moriyama, Analysis of adsorption behavior of cations onto quartz surface by electrical double-layer model, *J. Nucl. Sci. Technol.* 36 (1999) 1167–1175.
- [34] R. Venditti, X. Xuan, D. Li, Experimental characterization of the temperature dependence of zeta potential and its effect on electroosmotic flow velocity in microchannels, *Microfluid. Nanofluid.* 2 (2006) 493–499.
- [35] A.M. Gaudin, D.W. Fuerstenau, Quartz flotation with anionic collectors, *Trans. Am. Instit. Mining Metall. Eng.* 202 (1955) 66–72.
- [36] M. Wang, A. Revil, Electrochemical charge of silica surfaces at high ionic strength in narrow channels, *J. Colloid Interface Sci.* 343 (2010) 381–386.
- [37] R. Charmas, W. Piasecki, Four-layer complexation model for ion adsorption at electrolyte/oxide interface: interrelations of model parameters, *Langmuir* 12 (1996) 5458–5465.
- [38] R.J. Hunter, *Foundations of Colloid Science*, second ed., Oxford University Press, DOI, 2001.
- [39] A. Crespy, A. Boleve, A. Revil, Influence of the Dukhin and Reynolds numbers on the apparent zeta potential of granular porous media, *J. Colloid Interface Sci.* 305 (2007) 188–194.
- [40] T. Preočanin, W. Janusz, N. Kallay, Evaluation of equilibrium parameters of the anatase/aqueous electrolyte solution interface by introducing surface potential data, *Colloids Surf. A* 297 (2007) 30–37.
- [41] H. Yotsumoto, R.-H. Yoon, Application of extended DLVO theory: I. Stability of rutile suspensions, *J. Colloid Interface Sci.* 157 (1993) 426–433.
- [42] P. Leroy, C. Tournassat, M. Bizi, Influence of surface conductivity on the apparent zeta potential of TiO₂ nanoparticles, *J. Colloid Interface Sci.* 356 (2011) 442–453.
- [43] J.H. Masliyah, S. Bhattacharjee, *Electrokinetic and Colloid Transport Phenomena*, John Wiley & Sons, New Jersey, 2006. DOI.
- [44] I. Borukhov, D. Andelman, H. Orland, Steric effects in electrolytes: a modified Poisson-Boltzmann equation, *Phys. Rev. Lett.* 79 (1997) 435–438.
- [45] I. Borukhov, D. Andelman, H. Orland, Polyelectrolyte solutions between charged surfaces, *Europhys. Lett.* 32 (1995) 499–504.
- [46] J. Lyklema, J.T. Overbeek, On interpretation of electrokinetic potentials, *J. Colloid Sci.* 16 (1961). 501-&.